Publications

Available Online

J. Sci. Res. **15** (1), 261-274 (2023)

JOURNAL OF SCIENTIFIC RESEARCH

www.banglajol.info/index.php/JSR

The Study of Kinetics and Isotherms of Methylene Blue Adsorption onto Activated Carbon-Loaded Cellulose Composite Bead

P. Sarkar*

Department of Chemistry, Nabadwip Vidyasagar College, University of Kalyani, Nadia, West Bengal, India

Received 11 July 2022, accepted in final revised form 28 October 2022

Abstract

A novel adsorbent-activated carbon-loaded cellulose composite bead (AC-CCB) was synthesized by sol-gel conversion for the removal of methylene blue (MB) from an aqueous solution. The adsorbent was characterized by Fourier transform-infrared spectroscopy (FT-IR), field emission scanning electron microscope (FESEM), and X-ray energy dispersive spectroscopy (EDAX). The maximum dye removal was found to be 96.5, 92.3, and 81.8 %, corresponding to MB concentrations of 25, 50, and 100 $mgL^{-1,}$ respectively. Isotherm and the kinetic study were carried out with an AC-CCB dose of 1.0 g L^{-1}, a shaking speed of 125 rpm, and the initial MB concentration ranging from 25-100 mg L^{-1}. In order to study the kinetics of MB adsorption onto AC-CCB, the temperature was fixed at 298 K, whereas, for the isotherm study, the temperature varied from 298 to 318 K. The process followed pseudo-second-order kinetics with rate constant (k_2) $28.7x10^{-2}$, $11.1x10^{-2}$ and $9.41x10^{-2}$ $g.mg.min^{-1}$ corresponding to MB concentration of 25, 50 and 100 mg L^{-1}. Freundlich, Langmuir, and Sips models were found to fit well with the adsorption data. The negative ΔG^0 values and the positive ΔH^0 values suggested that the adsorption of MB onto AC-CCB was spontaneous and endothermic.

Keywords: Adsorption; Methylene blue; AC-CCB; Isotherms; Kinetics and thermodynamic parameters.

© 2023 JSR Publications. ISSN: 2070-0237 (Print); 2070-0245 (Online). All rights reserved.
doi: http://dx.doi.org/10.3329/jsr.v15i1.60717 J. Sci. Res. **15** (1), 261-274 (2023)

1. Introduction

Dyes are extensively used in several industries, viz., leather, cosmetics, pharmaceuticals, food processing, and textiles [1,2]. The use of synthetic dye is increasing day by day with the global population growth. Synthetic dye-consuming industries release a huge amount of unfixed dyes into the industrial effluent and it is a major environmental issue. So, removing these unfixed dyes from the industrial effluents or an aqueous solution is a major challenge to researchers. Several processes like advanced oxidation process (AOP) [3-5], coagulation-flocculation [6,7], reverse osmosis, dialysis/electrodialysis [8], nanofiltration [9], ultrafiltration [10] membrane separation [11], adsorption [12-15], etc. are employed for decontamination of sample matrix from synthetic dyes by the

* *Corresponding author*: pankaj@nvc.ac.in

researchers. The adsorption technique is preferred over other techniques for its simplicity, cost-effectiveness, feasibility, and recyclability. Methylene blue is a thiazine dye commonly used for dyeing materials, staining biological samples, and as a medication to treat methemoglobinemia. Methylene blue was first synthesized by Caro, a German chemist, in 1876 [16]. Moldenhauer [17] reported the use of methylene blue as an antidote for carbon monoxide and cyanide poisoning.

In the present study, the adsorption process was employed for the removal of methylene blue from an aqueous solution. Biological materials like cellulose are widely used for the removal or decontamination of synthetic dye from an aqueous solution because of their ease of availability and cost-effectiveness. Activated carbon is another important adsorbent used for the same purpose. In the present study, cellulose is converted to an activated carbon-impregnated cellulose composite bead (AC-CCB) via sol-gel conversion and is used for the removal of methylene blue.

2. Experimental

2.1. *Materials*

Analytical grade solvents and chemicals were purchased to prepare the adsorbent and perform the batch adsorption study. Cellulose powder and methylene blue were purchased from Merck, India. Activated carbon was purchased from Loba Chemie, India. 1000 mg L^{-1} stock solution of methylene blue was prepared by dissolving 1.0 g of MB in deionized water in a 1000 mL volumetric flask.

2.2. *Adsorption experiment*

The batch adsorption study was selected for the removal of MB from an aqueous solution. Initially, a definite amount of AC-CCB and 10 mL of dye solution were taken in a 100 mL conical flask. In order to achieve equilibrium, the conical flask was shaken in a rotary shaker (Remi 12R). The residual dye solution was centrifuged for 5 min at 3500 rpm, and the absorbance of the solution was measured by UV-VIS spectrophotometer (Shimadzu 1900i) at λ_{max} 665 nm. The percent removal of the dye solution was calculated by the following equation

$$Removal\ (\%) = \frac{C_0 - C_e}{C_0} \quad (1)$$

where C_0 is the initial dye concentration and C_e is the equilibrium dye concentration.

The batch adsorption study was performed by taking three different concentrations, viz., 25, 50, and 100 mg L^{-1}. The variation of shaking speed was carried out, ranging from 75 to 150 rpm. The effect of temperature was investigated at three different temperatures, viz., 298, 308, and 318 K. The solution pH was adjusted with 0.1 M NaOH and 0.1 M HCl solution. The equilibrium adsorption was achieved at 120 min of contact time, and the maximum dye removal was found to be 96.5, 92.3, and 81.8 %, corresponding to MB concentrations of 25, 50, and 100 mg L^{-1}, respectively.

3.3. *Preparation of adsorbent*

The noble adsorbent activated carbon-impregnated cellulose composite bead (AC-CCB) was prepared by the sol-gel approach. At first, 1.0 g of cellulose powder was soaked in 20 mL of 20 % NaOH solution for 48 h. A required volume of carbon disulfide was added to the cellulose-NaOH mixture, and the mixture was shaken for 6 h to obtain a clear solution. The mixture was shaken for another 3 h after the addition of 12.5 mL of 6 % NaOH solution. Then it was settled for 96 h at room temperature, and thereafter, a definite amount of activated carbon was added to the mixture. At the final stage, the mixture was added to methanol to obtain black colored activated carbon-loaded cellulose composite bead (AC-CCB) in a 250 mL beaker using a 5.0 mL syringe. The bead was washed several times with double distilled water and was stored in water in an air-tight container.

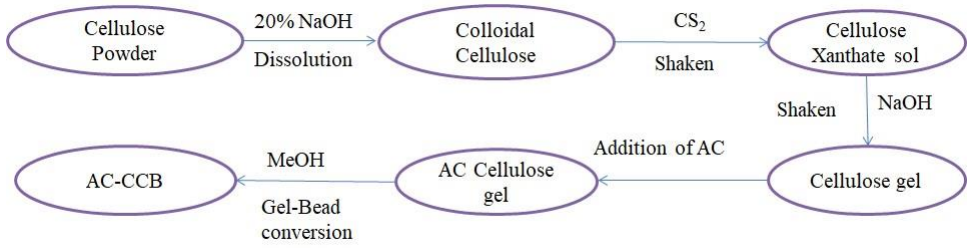

Scheme 1. Synthesis of AC-CCB.

3. Results and Discussion

3.1. *Characterization of adsorbent*

Characterization of adsorbent is one of the most important steps in a feasible adsorption process. The adsorbent AC-CCB was characterized by FTIR, FESEM, and EDS. The analysis of the topography of the adsorbent surface is very much important for a suitable adsorption process, as the adsorbate molecules get attached to the surface of the adsorbent. FTIR spectroscopy is used to determine the functional group of the material. In the present study, the synthesized AC-CCB was investigated within the frequency range of 450-4000 cm^{-1} (Fig. 1). Absorption bands at 3785 and 3409 cm^{-1} were attributed to stretching band of –OH in cellulose [18,19]. The absorption bands at 1380, 1161, 1058, and 895 cm^{-1} are assigned to C-H bending (in-plane) (1380 cm^{-1}), C-O-H bending at C-6 (1161 cm^{-1}), C-C, C-OH, C-H ring (1058 cm^{-1}) and C-O-C, C-C-O, C-C-H deformation and stretching (895 cm^{-1}) of cellulose [20]. A symmetrical C-H stretching band (in-plane) was found at 2922 cm^{-1}.

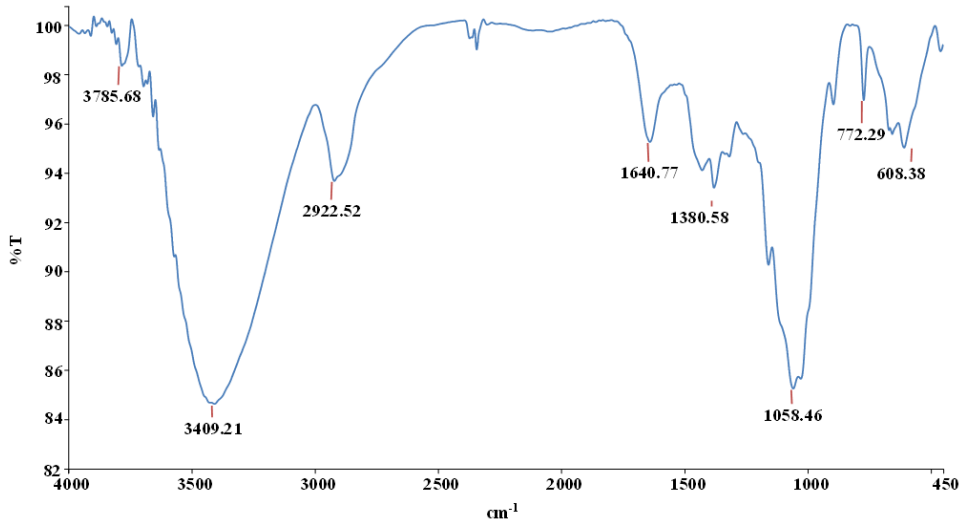

Fig. 1. FT-IR spectrum of AC-CCB.

In the present study, the topography of the AC-CCB surface was analyzed from the image obtained from a field emission scanning electron microscope (Make: Zeiss) with a voltage of 5.00 KV. Two different magnifications (25.00 KX and 50.00 KX) were chosen at the scale of 1 µm and 200 nm for imaging the sample. FESEM image revealed the presence of roughness and several pores on the AC-CCB surface. It might be concluded that the topographic structure of AC-CCB facilitated the adsorption of MB on the adsorbent surface.

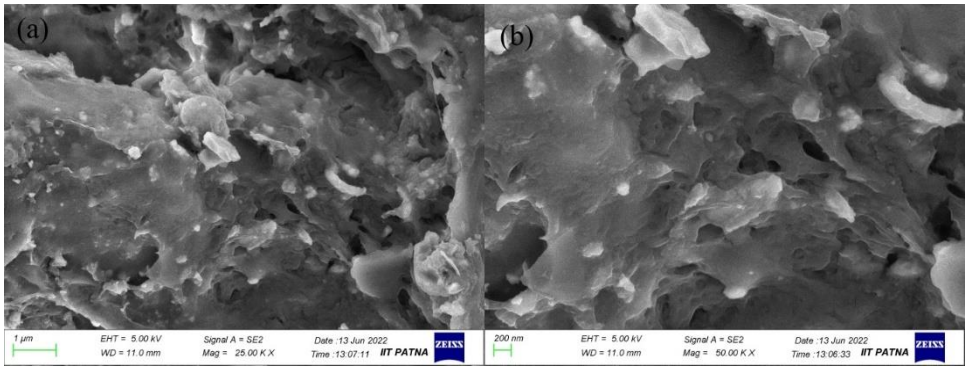

Fig. 2. FESEM of AC-CCB (a) 25.00 KX at a scale of 1 µm and (b) 50.00 KX at a scale of 200 nm.

Elemental detection was performed with X-ray energy dispersive spectroscopy (EDAX) coupled with a Zeiss field emission scanning microscope. The EDAX spectrum of the AC-CCB is represented in Fig. 3, and the elemental composition is represented in Table 1. The peaks of carbon and oxygen appeared in the EDAX spectrum of the AC-

CCB (Fig. 3) adsorbent. Table 2 represents the weight percent and atomic percent of carbon and oxygen in AC-CCB.

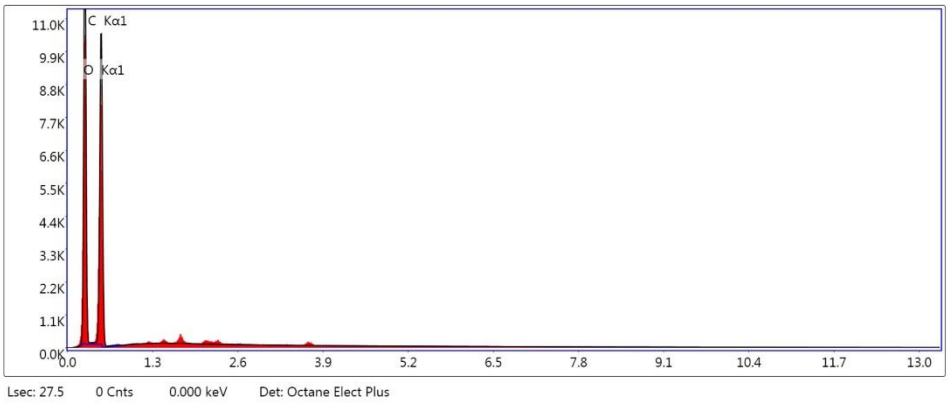

Fig. 3. EDAX spectrum of AC-CCB.

Table 1. Elemental composition of AC-CCB.

Element	Weight %	Atomic %	Error %
C K	48.75	55.89	5.37
O K	51.25	44.11	9.17

3.2. *Adsorption isotherm*

Adsorption isotherm can be defined as the amount of solute uptake onto the surface of the adsorbent at constant pressure or temperature. The study of isotherms provides information regarding the mechanism and surface characteristics of adsorbents of a feasible adsorption process. Adsorption isotherms are generally classified based on parameters involved in the adsorption process. In the present case, two-parameter and three-parameter isotherms viz. Langmuir, Freundlich, Temkin, Dubinin-Raduskevich, and Sips isotherms are studied for the removal of MB onto synthesized AC-CCB. The adsorption experiment was carried out with 1.0 g L^{-1} AC-CCB, an initial dye concentration ranging from 25 to 100 mg L^{-1}, an equilibrium time of 120 min, and a temperature ranging from 298 to 318 K.

3.2.1. *Langmuir isotherm model*

Langmuir's adsorption isotherm model can be used for both gaseous and solute particles in the liquid phase. The most important assumption of the model is that the monolayer adsorption occurs on the surface of the adsorbent, and no interaction between the solute particles on the adsorbent surface is considered. The linear form of the model can be represented as [21]

$$\frac{C_e}{q_e} = \frac{1}{q_m K_L} + \frac{C_e}{q_m} \quad (2)$$

where C_e (mg L^{-1}) is the equilibrium concentration, q_e (mg g^{-1}) is the amount of solute adsorbed at equilibrium, K_L (L mg^{-1}) is the Langmuir adsorption constant, and q_m (mg g^{-1}) is the maximum adsorption capacity. The values of q_m and K_L are calculated from the slope and intercept, respectively, of the plot of $\frac{C_e}{q_e}$ against C_e.

The plot of $\frac{C_e}{q_e}$ against C_e for the adsorption of MB onto AC-CCB is represented in Fig. 4. It was found that the adsorption data were well-fitted in the Langmuir model showing a linear regression value (R^2) close to unity at all the studied temperatures. According to the Langmuir isotherm model, the maximum adsorption capacity was found to be 0.933, 0.958, and 0.957 mg $g^{-1,}$ corresponding to the temperature of 298, 308, and 318 K, respectively. The value of Langmuir isotherm constant (K_L) was found to increase from 12.9 to 30.9 L mg^{-1}, with increasing temperature from 298 to 318 K.

3.2.2. *Freundlich isotherm model*

The adsorption of solute particles on heterogeneous surfaces can be explained by the Freundlich adsorption isotherm. It is employed in non-ideal and reversible multilayer adsorption systems [22]. The linear form of the isotherm can be represented as [22]

$$lnq_e = lnK_F + \frac{1}{n} lnC_e \quad (3)$$

where, K_F ($mg^{1-1/n}$ $L^{1/n}$ g^{-1})) is the Freundlich constant, C_e (mg L^{-1}) is the equilibrium dye concentration and n is related to adsorption energy distribution [22].

The plot of lnq_e against lnC_e of MB adsorption onto AC-CCB is represented in Fig. 4(b). The adsorption data were found to fit well with the Freundlich model. The values of 1/n were found to be 0.470, 0.439, and 0.398 (mg dm^{-3})$^{-1/n,}$ corresponding to temperatures 298, 308, and 318 K. The isotherm constant value was found to increase from 15.9 to 26.2 $mg^{(1-1/n)}$ $L^{1/n}$ g^{-1} with increasing temperature from 298 to 318 K.

3.2.3. *Temkin isotherm model*

This model is based on the assumption that the heat of adsorption of all molecules in the layer decreases linearly with an increase in surface coverage [23]. The linear form of the isotherm equation can be represented as [23]

$$q_e = \left(\frac{RT}{B_T}\right) lnA_T + \left(\frac{RT}{B_T}\right) lnC_e \quad (4)$$

where q_e (mg g^{-1}) and C_e (mg L^{-1}) represent the usual meanings. R is the universal gas constant, T (K) is the temperature at which the adsorption process is performed, A_T (L mg^{-1}) and B_T (J mol^{-1}) represents the adsorption capacity and the heat of adsorption, respectively. The plot of q_e against lnC_e is used to determine the isotherm constants A_T and B_T from the intercept and slope, respectively.

Fig. 4(c) represents the plot of the Temkin isotherm model of MB adsorption. The isotherm constant A_T was found to be 10.4, 2.03, and 3.77 L mg^{-1} while the value of B_T

was found to be $1.21x10^4$, $1.28x10^4$, $1.05x10^4$ J mol^{-1} corresponding to the temperature of 298, 308 and 318 K respectively.

3.2.4. *Dubinin-Raduskevich mode*l

Dubinin-Raduskevich model is mostly employed to determine the adsorption mechanism with a Gaussian energy distribution onto the heterogeneous adsorbent surface [24]. The isotherm equation can be represented as [25];

$$q_e = q_s exp(-K_{ad} \in^2) \quad (5)$$

where q_e (mg g^{-1}) is the amount of adsorbate onto the adsorbent, q_s (mg g^{-1}) is the theoretical isotherm saturation capacity, K_{ad} (mol K^{-1} J^{-1}) is the model constant, and ε is Polanyi potential which can be expressed as

$$\in = RTln\left(1 + \frac{1}{C_e}\right) \quad (6)$$

The linear form of the model can be expressed as

$$lnq_e = lnq_S - K_{ad} \in^2 \quad (7)$$

The values of K_{ad} and q_S can be determined from the slope and intercept, respectively, of the plot lnq_e against $\in^2$ (Fig. 4(d)). In the present study, the value of K_{ad} was found to be 0.124, 0.056, 0.039 mol K^{-1} $J^{-1,}$ and the theoretical isotherm saturation capacity (q_S) was found to be 0.607, 0.629, and 0.651 mg g^{-1} corresponding to temperature 298, 308 and 318 K.

The mean free energy of the adsorption process can be determined from the model constant K_{ad} using the following equation

$$E = (2K_{ad})^{-\frac{1}{2}} \quad (8)$$

The value of E< 8 suggests the process is physical adsorption, while E > 8 suggests chemical adsorption. In the present case, the value of mean free energy of the MB adsorption onto AC-CCB was 2.00, 2.98, and 3.58 KJ mol^{-1} corresponding to the temperature 298, 308, and 318 K, respectively, implying the physisorption nature of the process.

3.2.5. *Sips isotherm model*

Sips isotherm model is a three-parameter isotherm model which combines Langmuir and Freundlich models. The linear form of this equation is:

$$ln\frac{K_S}{q_e} = -\beta_s lnC_e + ln\, A_s \quad (9)$$

where K_s (L g^{-1}) is the Sips isotherm constant, β_s is the Sips isotherm model exponent and A_s (L mg^{-1}) is the Sips isotherm model constant. At low adsorbate concentration, the model reduces to the Freundlich model, whereas, at high adsorbate concentration, the model turns into the Langmuir model [26]. A plot of $ln\frac{K_S}{q_e}$ against $\ln C_e$ is used to

determine the value of β_s and A_s from the slope and intercept, respectively. Fig. 4(e) represents the plot of the Sips isotherm model of MB adsorption onto AC-CCB, considering the value of K_S =1.0 L g^{-1}. The value of the Sips isotherm exponent was found to decrease from 0.470 to 0.398 with increasing temperature from 298 to 318 K. The model constant was found to be 6.27, 4.91, and 3.81 L $mg^{-1,}$ corresponding to temperatures 298, 308, and 318 K, respectively.

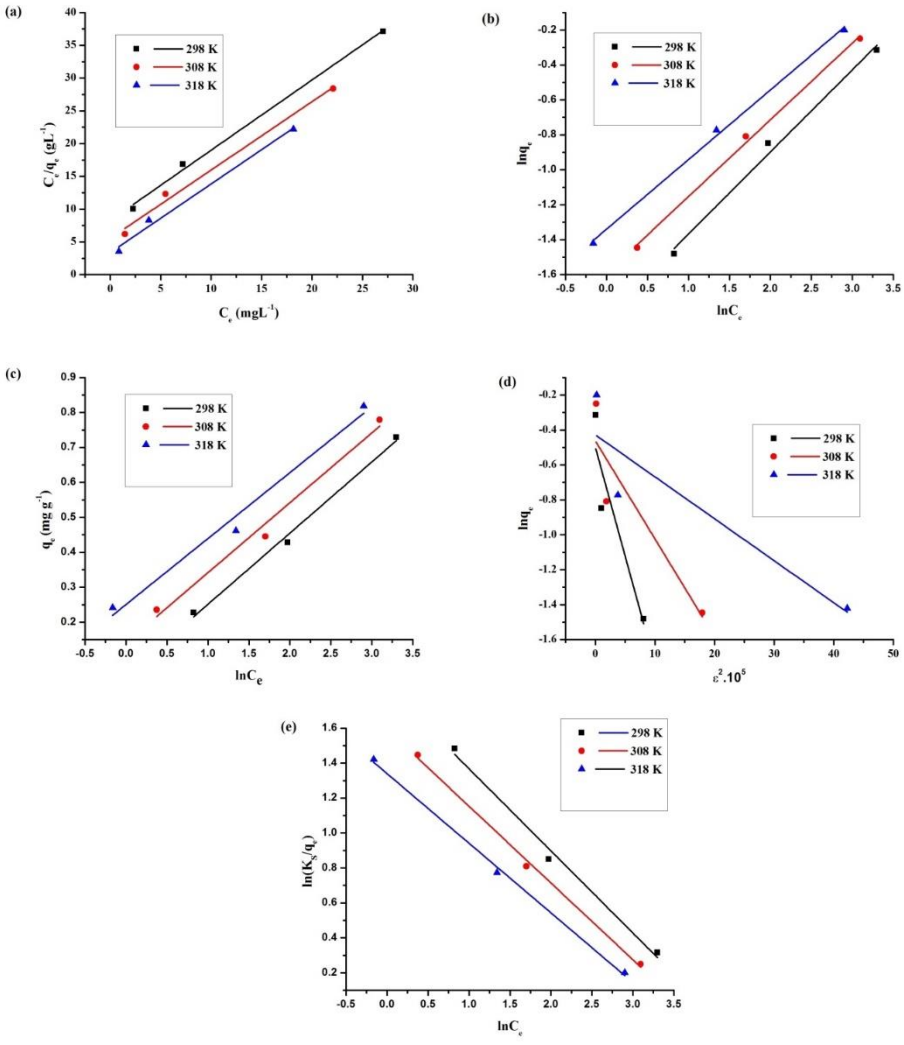

Fig. 4. Different adsorption isotherms (a) Langmuir, (b) Freundlich, (c) Temkin, (d) Dubinin-Raduskevich, and (e) Sips.

Table 2. Isotherm parameters.

Langmuir	T (K)	q_m (mg g^{-1})	$K_L.10^2$ (L mg^{-1})		R^2	S.E.
	298	0.933	12.9		0.997	1.09
	308	0.958	18.9		0.992	1.39
	318	0.957	30.9		0.992	1.19
Freundlich	T (K)	$K_F.10^2$(g mg^{-1})	1/n (mg $L^{-1})^{-1/n}$		R^2	S.E.
	298	15.9	0.470		0.991	0.074
	308	20.3	0.439		0.997	0.044
	318	26.2	0.398		0.987	0.040
Temkin	T (K)	A_T (L mg^{-1})	$B_T.10^{-4}$ (Jg mg^{-1} mol^{-1})		R^2	S.E.
	298	10.4	1.21		0994	0.026
	308	2.03	1.28		0.986	0.045
	318	3.77	1.05		0.984	0.051
D-R	T (K)	K_{ad}	q_s (mg g^{-1})		R^2	S.E.
	298	0.124	0.607		0.872	0.294
	308	0.056	0.629		0.849	0.329
	318	0.039	0.651		0.840	0.345
Sips	T (K)	K_s (L mg^{-1})	β_s	A_s (L mg^{-1})	R^2	S.E.
	298	1	0.470	6.27	0.991	0.074
	308	1	0.439	4.91	0.997	0.043
	318	1	0.398	3.81	0.998	0.040

3.3. *Kinetics of the adsorption*

In order to study the mechanistic pathway of adsorbent-solute interaction and rate-controlling step, a kinetic study of the adsorption process was carried out with 25, 50, and 100 mg L^{-1} MB solutions at 298 K, keeping the other equilibrium conditions constant. The kinetic data were analyzed using three different kinetic models: pseudo-first-order, pseudo-second-order, and intra-particle diffusion.

3.3.1. *Pseudo-first-order kinetics*

In the pseudo-first-order model, kinetic data were fitted to the following equation

$$\frac{dq_t}{dt} = k_1(q_e - q_t) \tag{10}$$

where q_e (mg g^{-1}) and q_t (mg g^{-1}) are the amounts of solute adsorbed onto the adsorbent surface at equilibrium and at the time 't', respectively. k_1 (min^{-1}) represents the rate constant of the adsorption process. Integration of the eq. (10) from t=0 to t=t yields the linear form of PFO model.

$$\ln(q_e - q_t) = lnq_e - k_1 t \tag{11}$$

The value of k_1 can be calculated from the slope of the plot of $\ln(q_e - q_t)$ against t.

In the present study, Fig. 5(a) represents the plot of $\ln(q_e - q_t)$ against t of the PFO model. The rate constant (k_1) was found to be 3.92×10^{-2}, 4.50×10^{-2} and 4.02×10^{-2} min^{-1} corresponding to MB concentration of 25, 50 and 100 mg L^{-1} respectively.

3.3.2. *Pseudo-second-order kinetics*

The rate equation of the pseudo-second-order (PSO) model can be expressed as eqn. (12) [27]

$$\frac{dq_t}{dt} = k_2(q_e - q_t)^2 \tag{12}$$

where k_2 is the rate constant of the PSO model. Integration of the above equation for limits t=0 to t=t and q_t=0 to q_t=t yields the linear form of the PSO model.

$$q_t = \frac{t}{\frac{1}{k_2 q_e^2} + \frac{t}{q_e}} \tag{13}$$

Eqn. (13) can be rearranged as [27]:

$$\frac{t}{q_t} = \frac{1}{k_2 q_e^2} + \frac{t}{q_e} \tag{14}$$

Fig. 5(b) represents the plot of t/q_t against t. The rate equation of the PSO model was determined from the intercept of the plot, while the amount of MB adsorbed onto the AC-CCB surface at equilibrium (q_e (mg g^{-1})) was determined from the slope of the plot. The linear regression values (R^2) of the PSO model were found to be more than 0.99 for all the studied concentrations indicating the suitable fitting of the data. The rate constants (k_2) were found to be 28.7×10^{-2}, 11.1×10^{-2} and 9.41×10^{-2} g mg min^{-1} corresponding to MB concentration of 25, 50 and 100 mg L^{-1}.

3.3.3. *Weber-Morris intra-particle (IP) diffusion*

The adsorption data were also analyzed using the Weber-Morris intra-particle (IP) diffusion model. The equation of the well-known IP model can be represented as eqn. (15) [24];

$$q_t = k_{id} t^{\frac{1}{2}} + C \tag{15}$$

where k_{id} (g mg^{-1} $min^{-1/2}$) is the rate constant of the IP model, and C is the intercept. Fig. 5(c) represents the plot of q_t against $t^{1/2}$ of MB adsorption onto AC-CCB. The initial curved portion of the plot is the film diffusion, i.e., the diffusion of MB molecules from the bulk solution to the AC-CCB surface, and the final linear portion of the plot indicates the intra-particle diffusion of MB molecules into the AC-CCB.

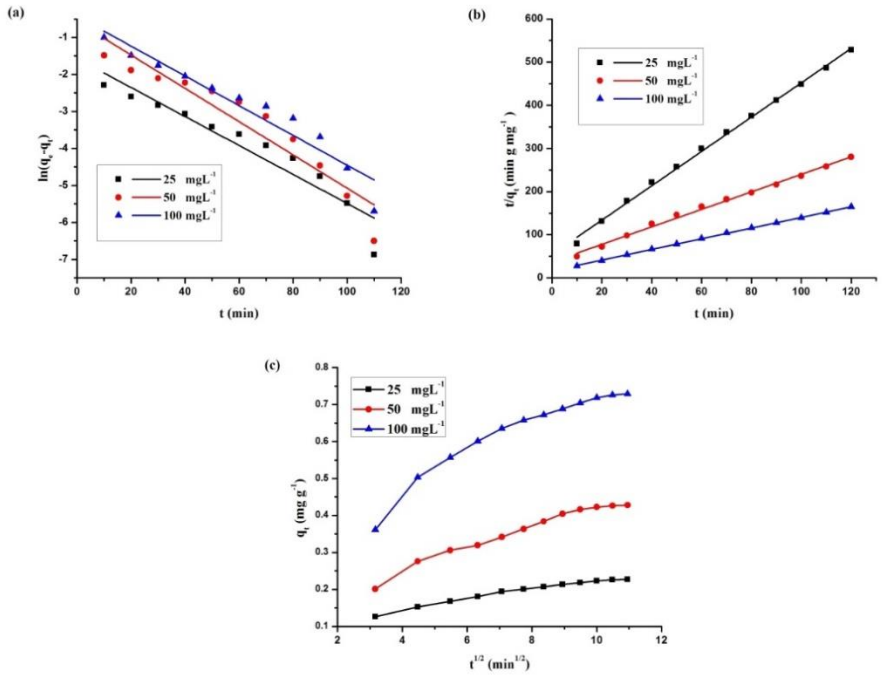

Fig. 5. Kinetic study of MB adsorption (a) pseudo-first-order, (b) pseudo-second-order, and (c) intra-particle diffusion.

Table 3. Kinetic parameters of MB adsorption onto AC-CCB.

	Conc. (mg L^{-1})	$k_1.10^2$ (min^{-1})	R^2	S.E.
PFO	25	3.92	0.907	0.438
	50	4.50	0.902	0.518
	100	4.02	0.929	0.390
	Conc. (mg L^{-1})	$k_2.10^2$ (g mg min^{-1})	R^2	S.E.
PSO	25	28.7	0.998	6.80
	50	11.1	0.995	5.25
	100	9.41	0.999	0.913
	Conc. (mg L^{-1})	$k_{id}.10^2$ (g mg^{-1} $min^{-1/2}$)	R^2	Intercept.10^2
IP	25	4.50	0.937	17.9
	50	5.40	0.957	36.9
	100	11.3	0.960	60.6

3.4. *Thermodynamic study*

The thermodynamic behavior of the adsorption of MB onto the AC-CCB surface was investigated by evaluating thermodynamic parameters, including changes in entropy, enthalpy, and Gibb's free energy. The spontaneity and feasibility of an adsorption process are related to Gibb's free energy change, ΔG^0. The negative value of ΔG^0 determines the

spontaneity of the process, and it is directly related to the equilibrium constant (K_c) of the adsorption process. In this study, K_c is determined by using the following equation:

$$K_c = \frac{C_a}{C_e} \tag{16}$$

where C_a (mg L^{-1}) and C_e (mg L^{-1}) are the amount of MB uptake at the AC-CCB surface and the concentration of MB on AC-CCB at equilibrium. The relation between K_c and ΔG^0 can be represented as

$$\Delta G^0 = -RTlnK_c \tag{17}$$

ΔG^0 is related to change in entropy (ΔS^0) and change in enthalpy (ΔH^0) by the following equation

$$\Delta G^0 = \Delta H^0 - T\Delta S^0 \tag{18}$$

By comparing eqn. (17) and eqn. (18),

$$RlnK_c = \Delta S^0 - \frac{\Delta H^0}{T} \tag{19}$$

The values of ΔS^0 and ΔH^0 can be calculated from the intercept and slope, respectively, by plotting $RlnK_c$ against $\frac{1}{T}$.

Fig. 6 represents the plot of $RlnK_c$ against $\frac{1}{T}$ for adsorption of MB onto the AC-CCB. The values of the studied thermodynamic parameters are represented in Table 4. All ΔG^0 values are found to be negative, suggesting the spontaneity of MB adsorption onto the AC-CCB surface. Positive ΔH^0 values suggest that the adsorption process is endothermic.

Table 4. Thermodynamic parameters.

Conc. of MB (mg L^{-1})	Temp. (K)	$-\Delta G^0$ (KJ mol^{-1})	ΔS^0 (KJ mol^{-1} K^{-1})	ΔH^0 (KJ mol^{-1})
25	298	5.52	0.157	41.26
	308	7.09		
	318	8.67		
50	298	4.30	0.108	27.88
	308	5.38		
	318	6.46		
100	298	2.40	0.076	20.25
	308	3.15		
	318	3.91		

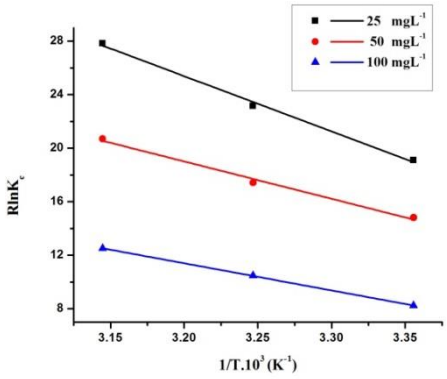

Fig. 6. Plot of $RlnK_c$ against 1/T.

4. Conclusion

The novel adsorbent AC-CCB was synthesized for the decontamination of methylene blue from an aqueous solution. The performance of the adsorbent towards the removal of MB was tested with different solute concentrations and the temperature ranging from 298-318 K. The adsorption isotherm, kinetics, and thermodynamic study were carried out to understand the characteristics and mechanism of the adsorption process. The kinetic study revealed that the adsorption data fitted well with pseudo-second-order kinetics. Both Langmuir and Freundlich models were found to fit well with the isotherm data. The studied three-parameter isotherm model, the Sips model, was also found to be an effective model. The negative values of change in Gibbs free energy confirm the spontaneity of the adsorption process, whereas the positive values of enthalpy indicate that the process is endothermic in nature.

Acknowledgment

The author wants to acknowledge the Department of Chemistry, Nabadwip Vidyasagar College, for infrastructural support and funding. The instrumental facilities received from IIT Patna and the University of Kalyani are duly acknowledged.

References

1. S. Khan and A. Malik, Environ. Sci. Pollut. Res. **25**, 4446 (2018). https://doi.org/10.1007/s11356-017-0783-7
2. M. T. Uddin, Y. Sultana, and M. A. Islam, J. Sci. Res. **8**, 399 (2016). https://doi.org/10.3329/jsr.v8i3.27524
3. P. Banerjee, S. Das Gupta, and S. De, J. Hazard. Mater. **140**, 95 (2007). https://doi.org/10.1016/j.jhazmat.2006.06.075
4. M. Pourgholi, R. Masoomi Jahandizi, M. Miranzadeh, O. H. Beigi, and S. Dehghan, Int. J. Environ. Sustain. Dev. **3**, 630 (2018).
5. S. Venkatesh, N. D. Pandey, and A. R. Quoff, IJARCSEIED **2**, 49 (2014).

6. S. S. Moghaddam, M. A. Moghaddam, and M. Arami, J. Hazard. Mater. **175**, 651 (2010). https://doi.org/10.1016/j.jhazmat.2009.10.058
7. Y. Y. Lau, Y. S. Wong, T. T. Teng, N. Morad, M. Rafatullah, and S. A. Ong, RSC Adv. **5**, 34206 (2015). https://doi.org/10.1039/C5RA01346A
8. M. Chen and C. T. Jafvert, Sep. Purif. Technol. **204**, 21 (2018). https://doi.org/10.1016/j.seppur.2018.04.053.
9. D. N. Yadav, K. Anand Kishore, and D. Saroj, Environ. Technol. **42**, 2968 (2021). https://doi.org/10.1080/09593330.2020.1720303
10. S. M. Doke and G. D. Yadav, Chemosphere **117**, 760 (2021). https://doi.org/10.1016/j.chemosphere.2014.10.029
11. R. V. Patel, G. B. Raj, S. Chaubey, and A. Yadav, Water Sci. Technol. **86**, 194 (2022). https://doi.org/10.2166/wst.2022.193
12. Y. Zhang, Y. Zheng, Y. Yang, J. Huang, A. R. Zimmerman, H. Chen, and B. Gao, Bioresour. Technol. **337**, ID 125432 (2021). https://doi.org/10.1016/j.biortech.2021.125432
13. I. Ghosh, S. Kar, T. Chatterjee, N. Bar, and S. K. Das, Process Saf. Environ. Prot. **149**, 345 (2021). https://doi.org/10.1016/j.psep.2020.11.003
14. B. T. Gemici, H. U. Ozel, and H. B. Ozel, Environ. Technol. Innov. **22**, ID 101501 (2021), https://doi.org/10.1016/j.eti.2021.101501
15. M. F. Imron, A. R. Ananta, I. S. Ramadhani, S. B. Kurniawan, and S. R. S. Abdull, Environ. Technol. Innov. **24**, ID 101921 (2021). https://doi.org/10.1016/j.eti.2021.101921
16. M. Wainwright and K. B. Crossley, J. Chemother. **14**, 431 (2002). https://doi.org/10.1179/joc.2002.14.5.431
17. M. Moldenhauer, JAMA **100**(1), 59 (1933). https://doi.org/10.1007/s11356-017-0783-7
18. A. Kingslin, K. Kalimuthu, and P. Viswanathan, J. Sc. Res. **14**, 343 (2022). https://doi.org/10.3329/jsr.v14i1.53782
19. P. Sarkar, S. Sarkar, D. Santra, S. Denrah, and M. Sarkar, FCE **3**, 133 (2022). https://doi.org/10.37256/fce.3220221541
20. M. Fan, D. Dai, and B. Huang, Fourier Transform Infrared Spectroscopy for Natural Fibers, in Fourier Transform – Materials Analysis, **3**, 45 (2012). https://doi.org/10.5772/35482
21. M. Munir, M. F. Nazar, M. N. Zafar, M. Zubair, M. Ashfaq, A. Hosseini-Bandegharaei, and A. Ahmad, ACS Omega **5**, 16711 (2020). https://doi.org/10.1021/acsomega.0c01613
22. N. Sharma, T. Alam, A. Rastogi, H. Tarannum, and G. Saini, J. Appl. Chem. **4**, 871 (2015).
23. N. Ayawei, A. N. Ebelegi, and D. Wankasi, J. Chem. **2017**, ID 3039817 (2017). https://doi.org/10.1155/2017/3039817
24. A. O. Dada, A. P. Olalekan, A. M. Olatunya, and O. J. I. J. C. Dada, IOSR-JAC **3**, 38 (2012).
25. E. M. Abd El-Monaem, A. M. Omer, G. M. El-Subruiti, M. S. MohY-Eldin, and A. S. Eltaweil, Biomass Conv. Bioref. (2022). https://doi.org/10.1007/s13399-022-02362-y
26. R. Sips, J. Chem. Phys. **16**, 490 (1948). https://doi.org/10.1063/1.1746922
27. H. Tsade Kara, S. T. Anshebo, F. K. Sabir, and G. A. Workineh, Int. J. Chem. Eng. **2021**, ID 9965452 (2021). https://doi.org/10.1155/2021/9965452